HYDROXYAPATITE/CARBON BASED BIOCOMPOSITE SCAFFOLDS AS PROSPECTIVE MATERIALS FOR BONE TISSUE ENGINEERING

Adrian Ionut NICOARA[1], Ionela Andreea NEACSU[1], Vladimir Lucian ENE[1], Bogdan Stefan VASILE[1], Anton FICAI[1], Ecaterina ANDRONESCU[1]

The purpose of this study was to obtain and characterize composite hydroxyapatite and graphene oxide-based materials for subsequent bone tissue regeneration applications. Synthesis of pure hydroxyapatite and samples with variable graphene oxide content were performed by microwave assisted hydrothermal method, thus obtaining dimensional homogeneous particles. The obtained powders were dispersed in polymer solutions (collagen, chitosan) and lyophilized in order to obtain porous structures. The resulting materials (powders and composites) were characterized morphologically, structurally and in-vitro.

Keywords: bone tissue engineering, collagen, chitosan, hydroxyapatite

1. Introduction

Due to its good biocompatibility and osteoconductive behavior, hydroxyapatite - $Ca_{10}(PO_4)_6(OH)_2$ - (HAp) is used in all forms (granular form, porous or dense bioceramics etc.) for bone reconstruction or substitution. The major drawback for using HAp in biomedical applications is represented by its low mechanical strength, therefore pure hydroxyapatite can be more suitable for drug delivery or restoration of low load-bearing areas, especially for cranio-maxillofacial tissues [1-2]. In order to design and obtain new HAp based materials for bone tissue regeneration with enhanced mechanical properties, different carbonaceous materials were recently investigated as reinforcement [3]. Carbon is a very abundant element on Earth and exists in each living organism. Studies show that different C allotropes forms (carbon nanotubes - CNT, diamond, graphene, graphite, graphene oxide – GO and buckyballs) exhibit biocompatibility (hence the usage for clinical applications such as artificial heart valves [4], bone fractures fixation devices [5], diabetic ulcers or skin wound dressings [6]) and good structural properties (high Young modulus, specific thermophysical and electrophysical properties), along with improving the fracture toughness of HAp [7]. When used in a small quantity, C tends to uniformly and evenly disperse into

[1] Faculty of Applied Chemistry and Materials Science, University POLITEHNICA of Bucharest, Romania, e-mail of corresponding author: neacsu.a.ionela@gmail.com

the ceramic matrix, acquiring mechanical strength enhancement for HAp-C based composites.

Graphene oxide (GO) consists of graphene sheets (monolayers of graphite) covered with oxygen-containing functional groups (-OH, -COOH etc.) on its planes and edges. Due to its large surface area (200-300 m^2g^{-1}) and wrinkled surfaces, a series of improvements emerge for the properties of GO reinforced bioceramics, such as hardness, fracture toughness and wear resistance. Along with all these benefits in using GO, its relative low cost of production makes it a suitable candidate for producing biomedical implants [8-10].

Porosity and flexibility are also important parameters to take into consideration when designing new materials for bone reconstruction. In the natural bone's structure, the flexibility is a result of the collagen fibrils with a diameter of 50-500 nm, which are interconnected with the apatite crystals and represent almost 90% of bone organic matrix [11-12].

In order to create biocomposites which mimic the structure of natural bone tissue, a series of natural and synthetic polymers are used, along with HAp [13]. Therefore, the most used natural polymer is collagen, a biocompatible natural material, multi-hierarchically structured, abundant, hydrophilic, easy to process and able to absorb high amount of body fluids, including exudate [14-15]. Its biomedical applications include skin regeneration dressings [16-17], bone [18-19], tendon and cartilage repair, drug delivery systems [20-22] and so on. The usage of collagen is limited by its poor physicochemical properties, including low resistance to enzymatic degradation. In order to address these limitations, the collagen modifications via crosslinking methods (physical, chemical or biochemical) is required, recently being under research natural cross-linkers, due to reduced toxicity [23-24].

Along with collagen, chitosan based biocomposites caught the attention recently for orthopedic tissue applications [25-26]. Also a natural polymer, chitosan is obtained by deacetylation of chitin, which is found in the exoskeleton of crustaceans, insects and mollusks. It possesses an intrinsic antimicrobial effect, therefore its applications in biomedical domain are far more interesting, because using it might reduce the risk of postsurgical infections [27-29].

Both collagen and chitosan can be used in porous form, after thermal processing [30-31]. The porous structure allows and encourages cell proliferation, thus faster tissue regeneration. Freeze drying method is used to create porous, three-dimensional polymeric or composite scaffolds, without affecting the structure of non-thermostable molecules. The obtained scaffolds mimic physically and structurally the natural tissue, being similar to extracellular matrix (ECM) [32].

The aim of this paper is to design and obtain porous freeze-dried biocomposite scaffolds based on graphene oxide reinforced hydroxyapatite (as

inorganic component) and collagen/chitosan (as natural polymers), thus mimicking the natural biocomposite, as prospective materials for bone tissue engineering.

2. Materials and methods

2.1 Graphene oxide synthesis

Graphene oxide was prepared according to the modified Hummer method: 20 g of graphite powder were magnetically stirred at 80^{o}C within a concentrated solution of H_2SO_4 (60 mL), $K_2S_2O_8$ (10 g) and P_2O_5 (10 g). The mixture was cooled to room temperature after which it was diluted with a large amount of water, filtered and washed until neutral pH. The obtained powder was dried for 24 hours at 80°C. 20 grams of pre-oxidized graphite was added over 460 mL of concentrated H_2SO_4 and the mixture was stirred in an ice bath (t <5°C) in a Berzelius beaker. To this mixture, 60 g of $KMnO_4$ were slowly added. After a few minutes, the Berzelius glass (in which a dark green solution was formed) was removed from the ice bath and placed on a magnetic stirring hood at 35°C inside the beaker for 2 hours. After heating, 920 mL distilled H_2O was poured in the mixture, and over 15 minutes the reaction was quenched by adding a large amount of distilled H_2O (2.8 L) and H_2O_2 30% (50 mL). The resulting mixture was decanted, filtered under vacuum, and washed with 5% HCl and distilled H_2O until neutral pH. The powder was then air dried for 24 h at 60^{o}C.

2.2 Hydroxyapatite/Graphene oxide hydroxyapatite synthesis

In a Berzelius beaker, $Ca(OH)_2$ and 100 mL of distilled water were added to form a slurry. In another Berzelius beaker, $(NH_4)_2HPO_4$ was dissolved in 20 mL distilled water. For samples with varying graphene oxide (GO) content (1%, 2% and 3%), graphene oxide previously obtained was dosed and dispersed by ultrasonication for 15 min in 20 mL of distilled water. After sonication, the mixture containing graphene oxide was dripped in the solution containing $Ca(OH)_2$ under continuous stirring, followed by the addition of the solution containing the phosphate, dropwise. The obtained mixtures were stabilized at pH 10 by adding ammonium hydroxide and placed in Teflon vessels inside the autoclave, for a microwave-assisted hydrothermal treatment of 20 minutes at 120°C and 2 bars pressure, then cooled to room temperature. Finally, the obtained precipitates were filtered, washed to neutral pH and allowed to dry overnight in the oven at 60°C. The resulted materials are further referred as HAp, HAp-1%GO, HAp-2%GO, HAp-3%GO.

2.3 Hydroxyapatite/Carbon based biocomposite scaffolds production

In order to obtain biocomposite scaffolds, the previously obtained powders (HAp, HAp–1%GO, HAp–2%GO and HAp–3%GO) were homogenously dispersed in polymer gels, the amount of used powder being based on the proportion of organic and inorganic materials in the bone composition, thus ensuring a mass ratio of 3:7. The collagen gel (1.46 wt% anhydrous substance, pH = 2.5) was supplied by Sanimed International Impex SRL, Romania. For the solubilization of chitosan, 6% acetic acid solution was used and the resulted mixture was sonicated for 30 minutes. The powders were dispersed in collagen/chitosan solutions under magnetic stirring until a uniform dispersion was formed. After stirring, the viscous solutions were sonicated for 15 minutes to remove the air bubbles. Glutaraldehyde 1% was added to collagen containing samples for further cross-linking overnight at 4^{o}C. Subsequently, in order to precipitate chitosan, a diluted solution of sodium hydroxide was added. Thus, the prepared gels were subjected to the freeze-drying process (freezing at 55°C for 12h, vacuum at 0.001 mbar for 12h and heating under vacuum for 24h to 35°C) in order to obtain porous composite materials. The resulted materials are further referred as HAp+Coll, HAp-1%GO+Coll, HAp-2%GO+Coll, HAp-3%GO+Coll, respectively HAp+CS, HAp-1%GO+CS, HAp-2%GO+CS, HAp-3%GO+CS. Also, reference collagen (Coll) and chitosan (CS) samples were obtained.

2.4 Characterization

X-ray diffraction analysis (XRD) was performed in order to characterize the materials synthesized from the point of view of their crystallinity as well as of the component phases. XRD analysis was performed using a PANalytrical Empyrean equipment in Bragg-Brentano geometry equipped with a Cu-anode ($\lambda CuK\alpha$ = 1.541874 Å) X-ray tube with in-line focusing, programmable divergent slit on the incident side and a programmable anti-scatter slit mounted on the PIXcel3D detector on the diffracted side. The analysis was acquired on the 20-80° angle range, with acquisition step of 0.02° and 100s acquisition time per step.

Scanning electron microscopy (SEM) was carried out to highlight morphological aspects of the synthesized samples and particle size. Image acquisition was performed using the High Resolution Scanning Electron Microscope, Inspect F50 at 30KeV with various magnification rates.

Transmission electron microscopy (TEM) images corresponding to graphene oxide were obtained using a high-resolution Tecnai G2 F30 S-TWIN transmission electron microscope equipped with a Selected Area Electron Diffraction (SAED) module. The microscope operated in bright-field transmission mode at a voltage of 300 kV, with a punctual and line resolution of 2 Å and 1 Å respectively.

The Fourier-transform infrared spectroscopy (FT-IR) investigation of the synthesized scaffolds implied the analysis of reduced sample quantities using the Nicolet iS50R spectrometer. Measurements were performed at room temperature using the Total Reflection Attenuation Module (ATR), with 32 sample scans between 4000 and 440 cm^{-1} at a resolution of 4 cm^{-1}. The recording of spectral data was possible by connecting the spectrometer to a data acquisition and processing unit through the Omnic program.

Raman spectra were recorded at room temperature in the range of 200 to 2000 cm^{-1}, using the green line of an Ar laser (λ = 514 nm) on a Horiba Jobin-Yvon LabRam HR spectrometer.

3. Results and discussions

3.1 Powder characterization

Fig. 1 shows the Raman spectra of GO (black), HAp–3%GO (green), HAp–2%GO (pink), HAp–1%GO (red) and HAp (blue). For GO there are two characteristic peaks in the spectra, the D band at 1353 cm^{-1} and the G band at 1590 cm^{-1}. The G band is related with the E_{2g} mode of graphite, which is usually associated to the in-phase vibrations of the graphite lattice, while the D band is assigned to the presence of vacancies, disorder and edges in the sp^2 network. In HAp+GO spectra were shown some characteristic peaks for HAp: 447 cm^{-1} (PO_4^{3-}), 598 cm^{-1} (PO_4^{3-}), and 958 cm^{-1} (PO_4^{3-}) respectively.

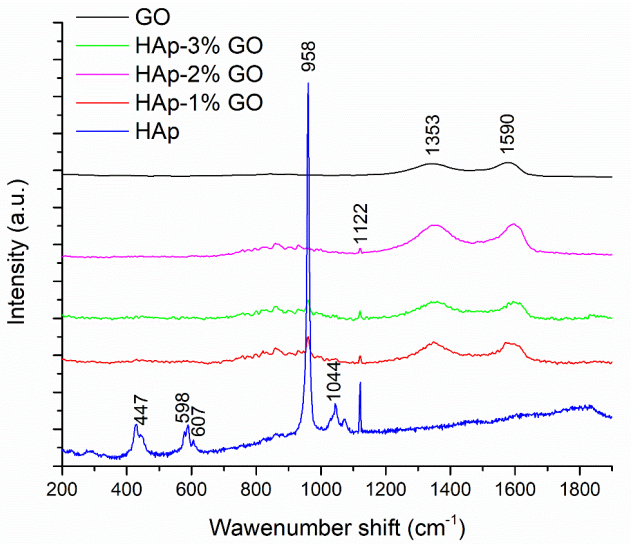

Fig. 1. Raman spectra of GO, HAp–3%GO, HAp–2%GO, HAp–1%GO and HAp

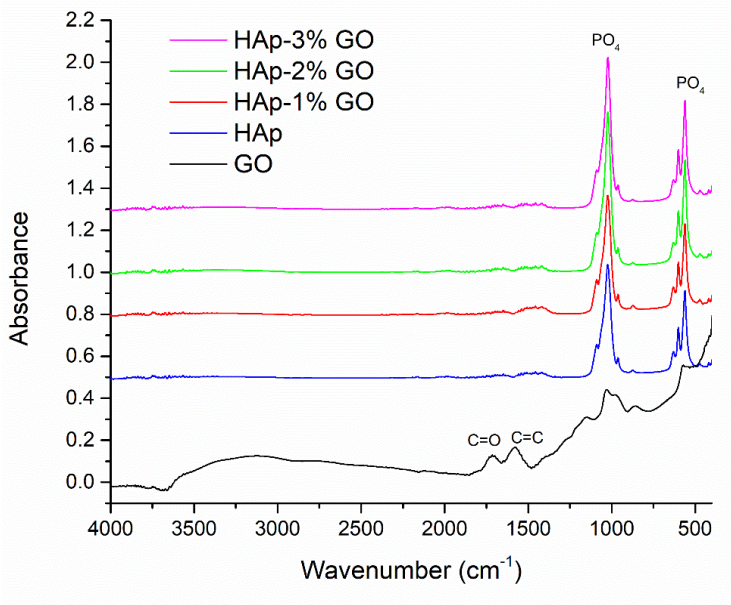

Fig. 2. FTIR spectra for HAp–3%GO, HAp–2%GO, HAp–1%GO, HAp and GO

The Fourier-transform infrared spectroscopy (FTIR) investigation was performed to verify GO reduction and functionalization with HAp nanoparticles, by the microwave-assisted hydrothermal method (Fig. 2). The characteristic absorption bands of GO, including alkoxy C–O stretching vibration groups (1023 cm^{-1}), epoxy C-O-C stretching vibration groups (1153 cm^{-1}) and C=O stretching vibration (1722 cm^{-1}), were identified. Further, a strong and broad absorption in region 3500-3000 cm^{-1}, due to O–H stretching vibrations, and an intense band at 1580 cm^{-1} corresponding to the C=C benzene ring mode were noticed [31]. As to the spectrum of prepared HAp, the bands at 1017 and 1091 cm^{-1} respectively correspond to the PO_4^{3-} asymmetric stretching, while the bands at 602 and 557 cm^{-1} are PO_4^{3-} antisymmetric deformation [32].

The XRD pattern of GO displayed the most intense peak at 2θ = 11.9° specific to the (001) plane (Fig. 3). Because of the attachment on both sides of the graphene sheet of oxygen-containing functional groups, as previously illustrated by FT-IR, GO has an average interlayer spacing of ~7.9A˚ [33]. The diffraction patterns show characteristic peaks of the HAp hexagonal phase, PDF4+ [01-080-6199]. Well-defined peaks appeared at 2θ around 25.9°, 31.9°, 32.9°, 34.1°, 39.8°, 46.7°, and 50.5°, which are attributed, respectively, to the (002), (211), (300), (202), (310), (222), and (321) reflections of HAp [34, 35].

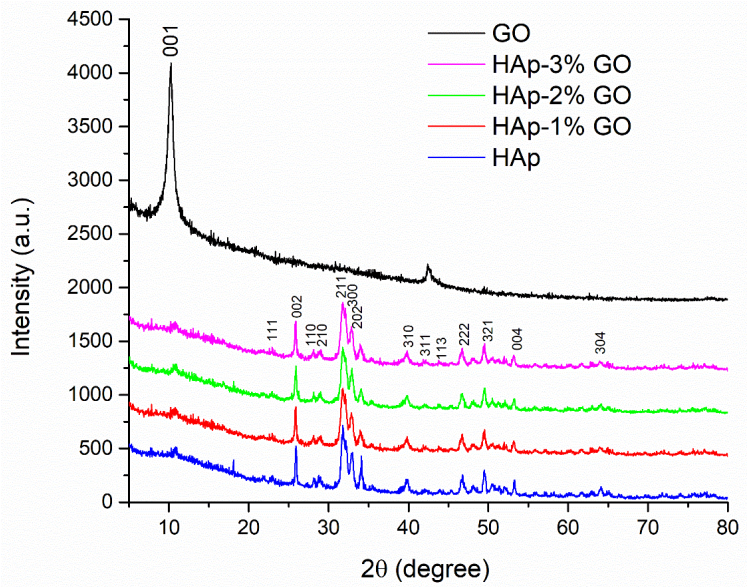

Fig. 3. XRD pattern of GO, HAp–3%GO, HAp–2%GO, HAp–1%GO and HAp

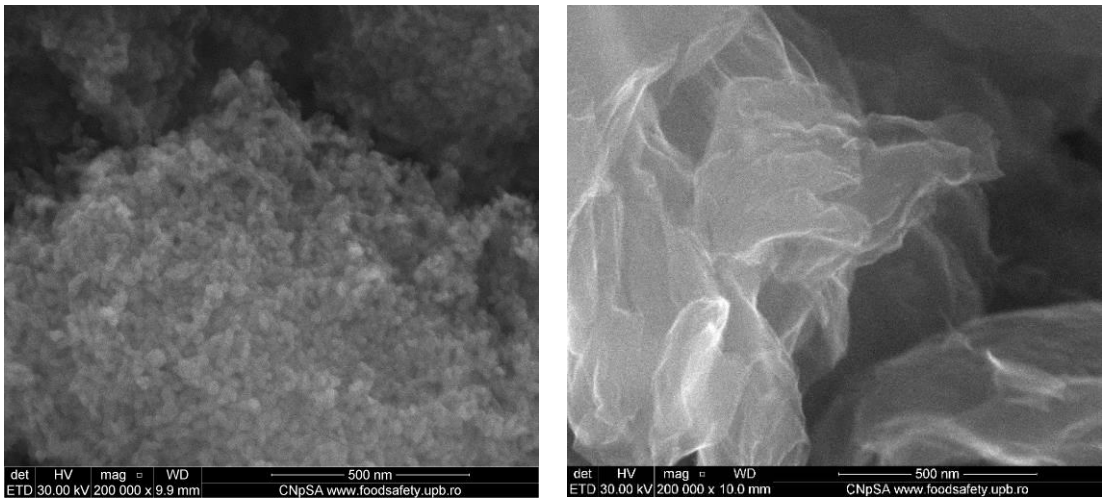

a) **b)**

Fig. 4. SEM images for a) HAp, b) GO.

In the case of hydroxyapatite sample, the obtained micrographs (Fig. 4 a) show the nanodimensional nature of the powder. The investigated sample has a quasi-spherical shape with particle sizes ranging from 12 to 30 nm. Due to its nanometric dimensions that lead to high specific surface, the powder is disposed in agglomerates. Based on the SEM images for GO powder (Fig. 4 b), one can observe the characteristic aspect of graphene oxide, represented by very thin sheets, folded and agglomerated, with lamellar morphology.

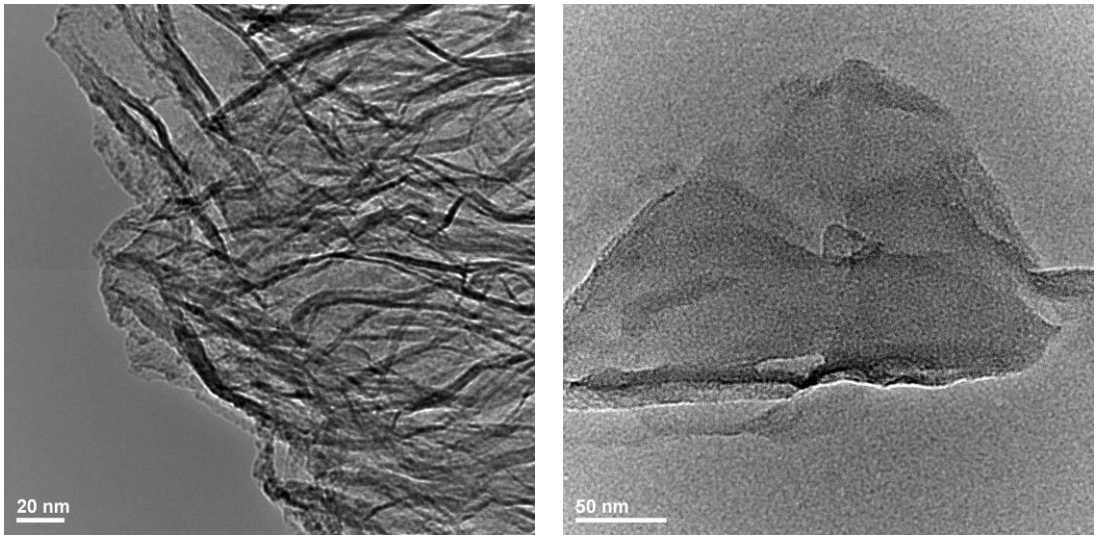

Fig. 5. TEM images for GO.

In Fig. 5, TEM images for GO are presented. It can be observed that the sheets identified also in SEM are formed by thin flat flakes. This is possible due to the sample preparation method for this specific analysis, meaning the dispersion in water of the powder and sonication for 15 min. Depending on the transparency degree, we can estimate that thin sheets of only a few layers of graphene oxide were formed.

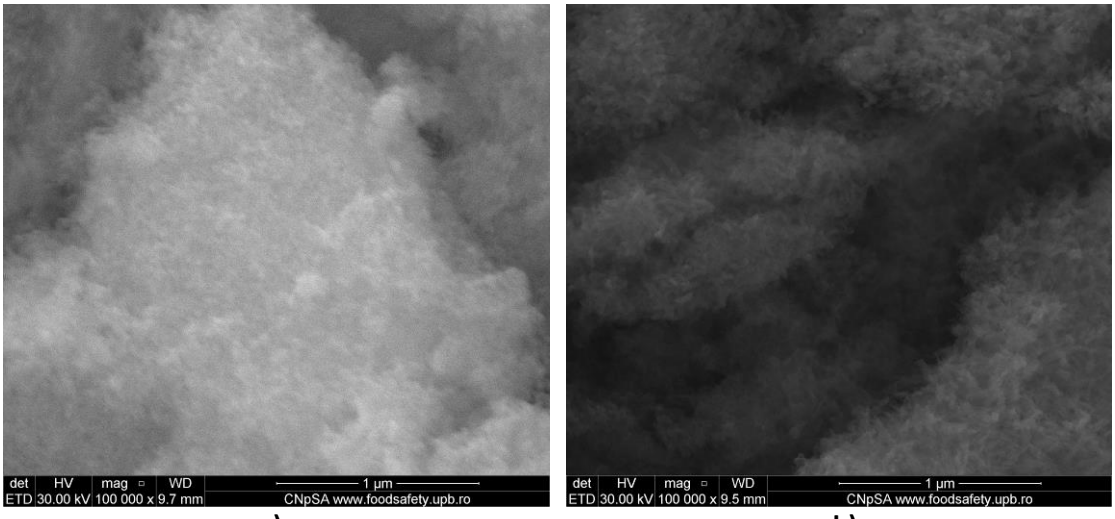

a) **b)**

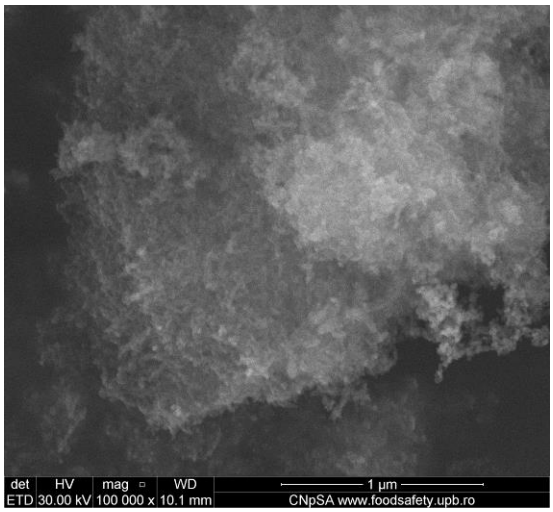

c)

Fig. 6. SEM images for HAp- GO composite materials: a) HAp–1%GO; b) HAp–2%GO; c) HAp–3%GO

Fig. 6 shows the powder micrographs for HAp–1%GO, HAp–2%GO and HAp–3%GO respectively. It can be noticed that the addition of graphene oxide did not significantly alter the HAp morphology previously identified, the obtained nanoparticles exhibiting mostly cvasi-spherical or elongated rounded shapes.

3.2 Biocomposite scaffolds characterization

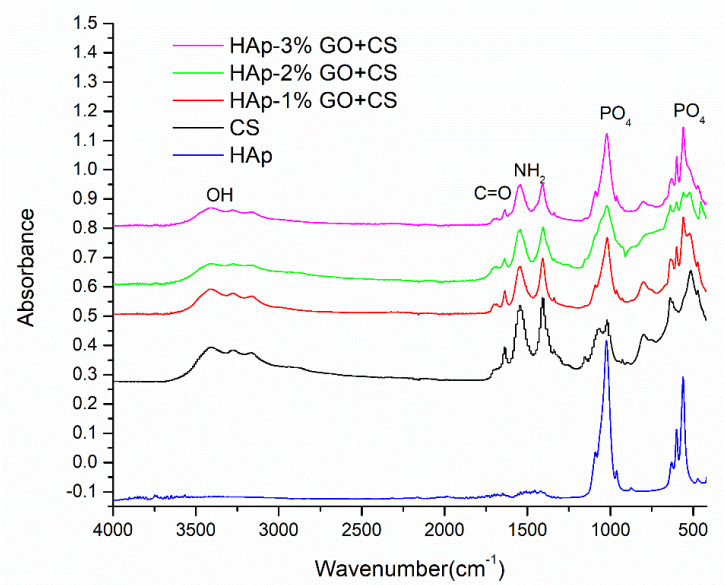

Fig. 7. FTIR spectra for HAp-3%GO+CS, HAp-2%GO+CS, HAp-1%GO+CS, CS and HAp

The FTIR spectra (Fig. 7) obtained for chitosan-based composites indicates the presence of several absorption bands. Thus, a strong band in the region 3421 cm^{-1} corresponds to N-H stretching vibration group. The presence of residual N-acetyl groups was confirmed by the bands at around 1650 cm^{-1} characteristic to C=O stretching of amide I and the small band at 1577 cm^{-1} corresponding to N-H bending of amide II. The characteristic band at 1409 cm^{-1} corresponds to hydroxyl group (-OH) and the absorption band at 1039 cm^{-1} can be attributed to asymmetric stretching of the C-O-C bond.

In the case of HAp-GO +CS the absorption band at 3450 cm^{-1} corresponds to the hydroxyl groups. The mineral phase, hydroxyapatite, can be observed by the presence of characteristic bands of PO_4^{3-} ion vibration, located in the low frequency range at 1036 cm^{-1}, 602 cm^{-1} and 566 cm^{-1}.

These specific bands decrease in absorbance with the addition and also the increase of graphene oxide content, which may be associated with poor interactions between system components. The existence of interactions is also suggested by flattening the broad band from the range of 3000-3500 cm^{-1} specific to the hydroxyl (-OH) groups of chitosan.

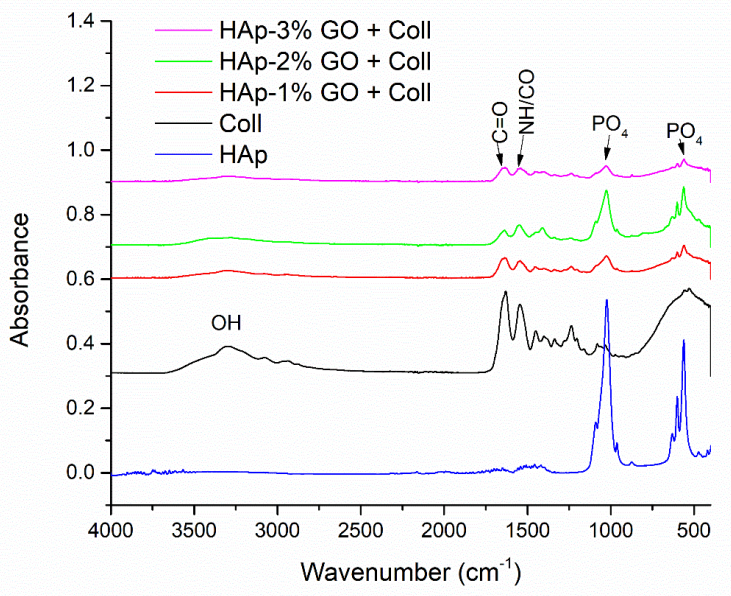

Fig. 8. FTIR spectra for HAp-3%GO+Coll, HAp-2%GO+Coll, HAp-1%GO+Coll, Coll and HAp

The presence of collagen can be demonstrated in all collagen-based composites by identification of its typical amide bands (A, B, I, II and III) in FTIR spectra (Fig. 8). Hence, the 1640 cm^{-1} area is attributed to the C=O elongation vibration of amide I coupled with the bending vibrations of the N-H bond and is representative for the secondary collagen structure, while the absorption band

from 1541 cm^{-1} corresponds to N-H amorphous deformation amide coupled to the stretching vibrations of the C-N bond. The amide absorption band III (1235 cm^{-1}) represents the combination of the maximum intensities between the deformation of the N-H bond and the C-N stretching vibrations. The amide absorption bands A (3306 cm^{-1}) and B (2964 cm^{-1}) resulted from the stretching vibrations of the N-H bond and the asymmetric stretch of the -CH_2 bond.

Also, on the composite spectra it was observed the presence of characteristic bands of PO_4^{3-} ion vibration, located in the low frequency range at 1030 cm^{-1} and 560 cm^{-1}. The same decrease in absorbance observed for chitosan based composites containing GO is also identified for collagen containing composites.

The SEM images presented in Fig. 9 show the porous morphology resulted from the freeze-dry process, similar for all obtained composites. The collagen (Fig. 9 a) is mainly formed by long intertwined fibers with diameter between 100 - 200 nm, uniformly distributed through the final materials. For the samples containing HAp, it can be observed in several areas how the particles are embedded in the collagen fibers matrix, unevenly distributed in the form of agglomerates with micrometric dimensions (Fig. 9 b). The sample based on chitosan presents a homogeneously distributed pore structure (Fig. 9 c) while for the samples containing chitosan and HAp, needle shaped particles crystalized at the surface (Fig. 9 d).

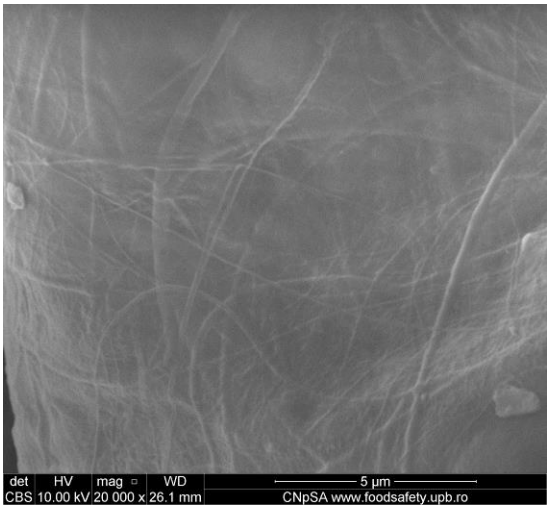

a)

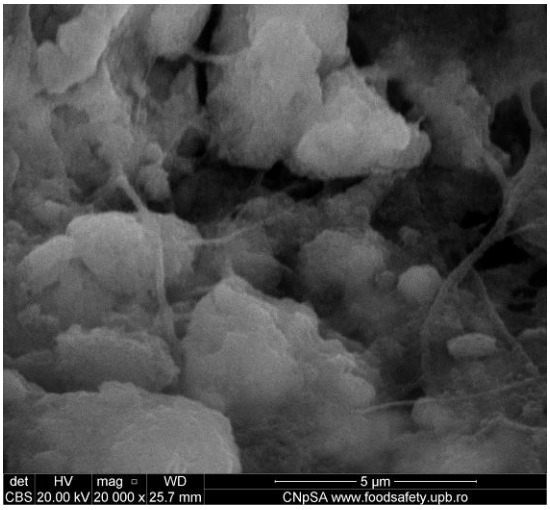

b)

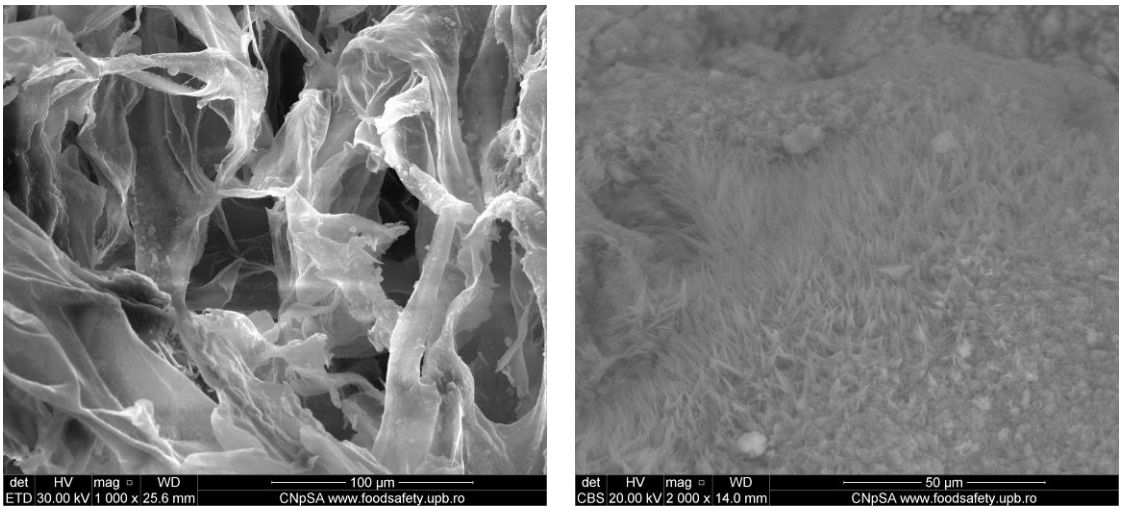

Fig. 9. SEM images for lyophilized samples: a) Coll, b) HAp-2% GO+Coll, c) CS and d) HAp-2% GO+CS

4. Conclusions

In order to achieve the desired goal, the synthesis and characterization of composite hydroxyapatite and graphene oxide-based materials for subsequent bone tissue regeneration applications, it was started from the production of graphene oxide by modified Hummers method, this being the most used in literature. The obtained powder was later characterized and used in the synthesis of graphene oxide containing hydroxyapatite, with various additive content from 1% to 3%, by the microwave-assisted hydrothermal method, which shortens the reaction time and has a much lower energy consumption than the classic hydrothermal method. For the biocomposites formation, 2 natural polymers were used, collagen and chitosan, and the porous morphology suitable for bone tissue regeneration was obtained by freeze drying process. All the obtained results regarding the graphene oxide formation into hydroxyapatite and the powders dispersion in the biocomposites, encourage us to further test the materials in order to demonstrate their ability to sustain osteoblastic function and formation of bone tissue.

Acknowledgement

We acknowledge with thanks the Academy of Romanian Scientists for their fully support.

REFERENCES

[1] *D. C. Lobb, B. R. DeGeorge, and A. B. Chhabra*, "Bone Graft Substitutes: Current Concepts and Future Expectations" Journal of Hand Surgery, Jan. 2019.

[2] *F. Raquel Maia, V. M. Correlo, J. M. Oliveira, and R. L. Reis*, "Natural Origin Materials for Bone Tissue Engineering: Properties, Processing, and Performance," Princ. Regen. Med., Jan. 2019, pp. 535–558.

[3] *H. A. Siddiqui, K. L. Pickering, and M. R. Mucalo*, "A review on the use of hydroxyapatite- carbonaceous structure composites in bone replacement materials for strengthening purposes," Materials (Basel)., vol. **11,** no. 10, 2018, pp. 1–32.

[4] *M. Namdari and A. Eatemadi*, "Nanofibrous bioengineered heart valve—Application in paediatric medicine," Biomed. Pharmacother., vol. **84**, Dec. 2016, pp. 1179–1188.

[5] *D. Nurettin and B. Burak*, "Feasibility of carbon-fiber-reinforced polymer fixation plates for treatment of atrophic mandibular fracture: A finite element method," J. Cranio-Maxillofacial Surg., vol. **46**, no. 12, Dec. 2018, pp. 2182–2189.

[6] *M. Nowacki et al.,* "New application of carbon nanotubes in haemostatic dressing filled with anticancer substance," Biomed. Pharmacother., vol. **69**, Feb. 2015, pp. 349–354.

[7] *T. T. Madanagopal, S. V. Agarwalla, and V. Rosa*, "Carbon nanocomposites for implant dentistry and bone tissue engineering," Appl. Nanocomposite Mater. Dent., Jan. 2019, pp. 47–63.

[8] *N. Shadjou, M. Hasanzadeh, and B. Khalilzadeh*, "Graphene based scaffolds on bone tissue engineering," *Bioengineered*, vol. **9**, no. 1, 2018, pp. 38–47.

[9] *S. Prasadh, S. Suresh, and R. Wong*, "Osteogenic Potential of Graphene in Bone Tissue Engineering Scaffolds," Materials (Basel)., vol. **11**, no. 8, Aug. 2018, p. 1430.

[10] *Y. Liu, N. Fang, B. Liu, L. Song, B. Wen, and D. Yang*, "Aligned porous chitosan/graphene oxide scaffold for bone tissue engineering," Mater. Lett., vol. **233**, Dec. 2018, pp. 78–81.

[11] *I. A. Neacşu, A. I. Nicoară, O. R. Vasile, and B. S. Vasile*, "Inorganic micro- and nanostructured implants for tissue engineering," in Nanobiomaterials in Hard Tissue Engineering, vol. **4**, 2016, pp. 271–291.

[12] *L. C. Palmer, C. J. Newcomb, S. R. Kaltz, E. D. Spoerke, and S. I. Stupp*, "Biomimetic Systems for Hydroxyapatite Mineralization Inspired By Bone and Enamel," Chem. Rev., vol. **108**, no. 11, 2008, p. 4754.

[13] *K. D. Park, X. Wang, J. Y. Lee, K. M. Park, S. Zhang, and I. Noh*, "Research trends in biomimetic medical materials for tissue engineering: commentary," Biomater. Res., vol. **20**, no. 1, 2016, p. 8.

[14] *J. Venkatesan and S. K. Kim*, "Nano-hydroxyapatite composite biomaterials for bone tissue engineering - A review" J. Biomed. Nanotechnol., vol. **10**, no. 10, 2014, pp. 3124–3140.

[15] *S. Preethi Soundarya, A. Haritha Menon, S. Viji Chandran, and N. Selvamurugan*, "Bone tissue engineering: Scaffold preparation using chitosan and other biomaterials with different design and fabrication techniques," International Journal of Biological Macromolecules, vol. **119**, Nov. 2018, pp. 1228–1239.

[16] *G. Pəunica-Panea et al.,* "New Collagen-Dextran-Zinc Oxide Composites for Wound Dressing," J. Nanomater., vol. **2016**, 2016.

[17] *D. A. Gyles, L. D. Castro, J. O. C. Silva, and R. M. Ribeiro-Costa*, "A review of the designs and prominent biomedical advances of natural and synthetic hydrogel formulations," European Polymer Journal, vol. **88**, Mar. 2017, pp. 373–392.

[18] *A. Ficai, E. Andronescu, D. Ficai, M. Sonmez, I. A. Nedelcu, and M. G. Albu*, "Collagen-based bone grafts, calcium phosphate and zinc and their preparation process," RO129822-A2, 2013.

[19] *I. L. Ardelean et al.*, "Collagen/hydroxyapatite bone grafts manufactured by homogeneous/heterogeneous 3D printing," Mater. Lett., vol. 231, Aug. 2018, pp. 179–182.
[20] *B. An, Y. S. Lin, and B. Brodsky*, "Collagen interactions: Drug design and delivery," Advanced Drug Delivery Reviews, vol. **97**, Feb. 2016, pp. 69–84.
[21] *S. Mondal et al.*, "Rapid microwave-assisted synthesis of gold loaded hydroxyapatite collagen nano-bio materials for drug delivery and tissue engineering application," Ceram. Int., vol. **45**, no. 3, Feb. 2019, pp. 2977–2988.
[22] *J. Jacob, J. T. Haponiuk, S. Thomas, and S. Gopi*, "Biopolymer based nanomaterials in drug delivery systems: A review" Materials Today Chemistry, vol. **9**, Sep. 2018, pp. 43–55.
[23] *T. Du, X. Niu, Z. Li, P. Li, Q. Feng, and Y. Fan*, "Crosslinking induces high mineralization of apatite minerals on collagen fibers," Int. J. Biol. Macromol., vol. **113**, Jul. 2018, pp. 450–457.
[24] *J. Kozłowska and A. Sionkowska*, "Effects of different crosslinking methods on the properties of collagen-calcium phosphate composite materials," Int. J. Biol. Macromol., vol. **74**, Mar. 2015, pp. 397–403.
[25] *M. A. S. Munhoz, H. H. Hirata, A. M. G. Plepis, V. C. A. Martins, and M. R. Cunha*, "Use of collagen/chitosan sponges mineralized with hydroxyapatite for the repair of cranial defects in rats," Injury, vol. **49**, no. 12, Dec. 2018, pp. 2154–2160.
[26] *S. Saravanan, R. S. Leena, and N. Selvamurugan*, "Chitosan based biocomposite scaffolds for bone tissue engineering," Int. J. Biol. Macromol., vol. **93**, Dec. 2016, pp. 1354–1365.
[27] *M. Ahmad, K. Manzoor, and S. Ikram*, "Chitosan nanocomposites for bone and cartilage regeneration," in Applications of Nanocomposite Materials in Dentistry, Woodhead Publishing, 2018, pp. 307–317.
[28] *Y. H. Chen, H. Y. Tai, E. Fu, and T. M. Don*, "Guided bone regeneration activity of different calcium phosphate/chitosan hybrid membranes," Int. J. Biol. Macromol., vol. **126**, Apr. 2019, pp. 159–169.
[29] *K. Pal et al.*, "Antimicrobial and biocompatible fluorescent hydroxyapatite-chitosan nanocomposite films for biomedical applications," Colloids Surfaces B Biointerfaces, vol. **171**, Nov. 2018, pp. 300–307.
[30] *P. C. Kavitha Sankar, G. Rajmohan, and M. J. Rosemary*, "Physico-chemical characterisation and biological evaluation of freeze dried chitosan sponge for wound care," Mater. Lett., vol. **208**, Dec. 2017, pp. 130–132.
[31] *M. C. Varley, S. Neelakantan, T. W. Clyne, J. Dean, R. A. Brooks, and A. E. Markaki*, "Cell structure, stiffness and permeability of freeze-dried collagen scaffolds in dry and hydrated states," Acta Biomater., vol. **33**, Mar. 2016, pp. 166–175.
[32] *Z. Fereshteh*, "Freeze-drying technologies for 3D scaffold engineering," in Functional 3D Tissue Engineering Scaffolds: Materials, Technologies, and Applications, Woodhead Publishing, 2017, pp. 151–174.
[33] *G. Wang et al.*, "Facile Synthesis and Characterization of Graphene Nanosheets," J. Phys. Chem. C, vol. **112**, no. 22, Jun. 2008, pp. 8192–8195.
[34] *I. Mobasherpour, M. S. Heshajin, A. Kazemzadeh, and M. Zakeri*, "Synthesis of nanocrystalline hydroxyapatite by using precipitation method," J. Alloys Compd., vol. **430**, no. 1–2, Mar. 2007, pp. 330–333.
[35] *M. Jevtić, M. Mitrić, S. Škapin, B. Jančar, N. Ignjatović, and D. Uskoković*, "Crystal Structure of Hydroxyapatite Nanorods Synthesized by Sonochemical Homogeneous Precipitation," Cryst. Growth Des., vol. **8**, no. 7, Jul. 2008, pp. 2217–2222.
[36] *C. Nethravathi and M. Rajamathi*, "Chemically modified graphene sheets produced by the solvothermal reduction of colloidal dispersions of graphite oxide," Carbon N. Y., vol. **46**, no. 14, Nov. 2008, pp. 1994–1998.